

IDENTIFICATION OF ANTI-CANCEROUS DRUGS FOR THE MUTATED SNAP25 PROTEIN RELATED TO BRAIN TUMOR THROUGH STRUCTURE-BASED VIRTUAL SCREENING APPROACH

POOJA PARASHAR, SAMEER SHARMA

Department of Bioinformatics, BioNome, Bengaluru, Karnataka, India. Email: info@bionome.in

Received: 30 January 2023, Revised and Accepted: 15 February 2023

ABSTRACT

Objective: Brain tumor is a formidable challenge for drug development, and drugs derived from many advanced technologies are being tested in clinical trials. Synaptosomal-associated protein of 25 kDa (SNAP25) is a membrane-binding protein in neurons and it is critical in neurotransmission for the fusion of plasma membrane and synaptic vesicle making it a prime target to address brain tumors. The SNAP-25 gene is responsible for personality disorders, schizophrenia, attention deficit, and hyperactivity disorder in human beings. It is recently discovered, that this protein is responsible for brain cancer as well.

Methods: In the present research, 17 investigational and experimental anticancer drugs were selected from the PubChem and DrugBank databases to identify potential inhibitors with high stability to treat mutated SNAP25 protein. For this purpose, we have used the structure-based virtual screening technique wherein, the candidate molecules are computationally docked into the 3D structure of the biological. The docking was achieved in PyRx 0.8 software and the drugs were then ranked based on their predicted binding affinity or complementarity to the binding site.

Results: Based on the ligand binding energy, the top six compounds having greater inhibitory effects towards SNAP25 were selected and then visualized with Pymol and Biovia visualizers. The compound Crenolanib has better pharmacological properties and demonstrated higher binding affinities with the target protein. Therefore, this Crenolanib docked confirmations were appraised for molecular dynamic simulations.

Conclusion: The study concluded that the anticancer drug Crenolanib exerted inhibitory potential against the mutated protein SNAP-25 and therefore it can be exploited as a cancer modulator to address brain tumors.

Keywords: Anti-cancer, Computer-aided drug design, Drug discovery, Structure-based virtual screening, AutoDock.

© 2023 The Authors. Published by Innovare Academic Sciences Pvt Ltd. This is an open access article under the CC BY license (<http://creativecommons.org/licenses/by/4.0/>) DOI: <http://dx.doi.org/10.22159/ijms.2023v11i2.47146>. Journal homepage: <https://innovareacademics.in/journals/index.php/ijms>

INTRODUCTION

Brain tumor, known as an intracranial tumor, is an abnormal mass of tissue in which cells grow and multiply uncontrollably, seemingly unchecked by the mechanisms that control normal cells. More than 150 different brain tumors have been documented, but the two main groups of brain tumors are termed primary and metastatic. Primary brain tumors include tumors that originate from the tissues of the brain or the brain's immediate surroundings. Primary tumors are categorized as glial (composed of glial cells) or non-glial (developed on or in the structures of the brain, including nerves, blood vessels, and glands) and benign or malignant. Metastatic brain tumors arise elsewhere in the body (such as the breast or lungs) and migrate to the brain, usually through the bloodstream. These tumors are considered cancer and are malignant. Brain tumors are thought to arise when certain genes on the chromosomes of a cell are damaged and no longer function properly. In some cases, an individual may be born with partial defects in one or more of these genes. Environmental factors may then lead to further damage. Once a cell is dividing rapidly and internal mechanisms to check its growth are damaged, the cell can eventually grow into a tumor. Tumors may produce substances that block the immune system from recognizing the abnormal tumor cells and eventually overpower all internal and external deterrents to its growth.

It is already known, that brain tumors are among the most fatal of all forms of cancer. More than two-thirds of adults diagnosed with glioblastoma, the most aggressive type of brain cancer will die within 2 years of diagnosis [1,2]. Brain cancers are also the most common and most lethal of all pediatric solid tumors [3]. These tumors have proved challenging to treat, largely due to the biological characteristics of these cancers, which often conspire to limit progress. These tumors

are located behind the blood-brain barrier (BBB) — a system of tight junctions and transport proteins that protect delicate neural tissues from exposure to factors in the general circulation, thus also impeding exposure to systemic chemotherapy [4,5]. Furthermore, the unique developmental, genetic, epigenetic, and microenvironmental features of the brain frequently render these cancers resistant to conventional and novel treatments alike [6-8].

Treatment options depend on several factors, such as the size, type, and grade of the tumor; if the tumor has spread to other parts of the CNS or body; possible side effects; the patient's preferences and overall health. It also includes surgery, radiation therapy, chemotherapy, and targeted therapy [7]. For low-grade brain tumors, surgery may be the only treatment needed, especially if all of the tumors can be removed. If visible tumors are remaining after surgery, radiation therapy and chemotherapy may be used. For higher-grade tumors, treatment usually begins with surgery, followed by radiation therapy and chemotherapy. Treatments using medication are used to destroy cancer cells. Medication may be given through the bloodstream to reach cancer cells throughout the body. When a drug is given this way, it is called systemic therapy. Medication may also be given locally, which is when the medication is applied directly to cancer or kept in a single part of the body. Therefore, types of medications used for brain tumors include chemotherapy and targeted therapy.

Some of the drugs frequently used for the treatment of brain tumors are better at going through the BBB: Carmustine, Citalopram, Belzutifan, Etoposide, Lomustine, Methotrexate, Temozolomide, etc. There have been different treatment procedures for every drug in combination with other cancer therapies, for example, gliadel wafers are a way to give the drug carmustine (BiCNU). These wafers are placed in the area where

the tumors were removed during surgery. For people with glioblastoma and high-grade glioma, the latest standard of care is radiation therapy with daily low-dose temozolomide. A combination of 3 drugs, lomustine (Gleostine), procarbazine (Matulane), and vincristine (Vincasar), has been used along with radiation therapy [8].

At present, bioinformatic analysis is being widely replicated in the field of cancer research, which saves the necessity of conducting experiments [9,10]. Accordingly, the process of identification of new cancer-treating drugs is very complex, expensive, and time-consuming, thus, computer-aided drug design approaches have been recognized as an alternative to overcome this situation [11-13]. Among these approaches, structure-based virtual screening (SBVS) [14-17] using molecular docking study [18,19] has become a valuable primary step in the identification of novel lead molecules for anticancer drug discovery. The process of computational docking starts with a target of known structure, such as a crystallographic structure of an enzyme of medicinal interest. Docking is then used to predict the bound conformation and binding free energy of small molecules to the target. Single docking experiments are useful for exploring the function of the target, and virtual screening, where a large library of compounds are docked and ranked, may be used to identify new inhibitors for drug development.

The protein studied in this review is synaptosomal-associated protein of 25 kDa (SNAP25) is a membrane-binding protein in neurons [20], which is recently discovered as a tumor suppressor of glioblastoma. This protein contributes to the plasma membrane and synaptic vesicle. SNAP-25 forms complexes with synaptobrevin in synaptic vesicles and with syntaxin in the plasma membrane. In simple terms, SNAP-25 protein is critical in neurotransmission for the fusion of plasma membrane and synaptic vesicle. Several studies investigated the relationship between SNAP-25 gene polymorphism and personality disorders, schizophrenia, attention deficit, and hyperactivity disorder.

In recent research, it was found that the SNAP25 level of expression was decreased in glioma tissues and cell lines, and low-level SNAP25 indicated an unfavorable prognosis for glioma patients. The protein inhibited cell proliferation, migration, and invasion and fostered glutamine metabolism of glioma cells, exerting a tumor suppressor role. Its overexpression exerted a lower expression level of MAP2, indicating poor neuronal plasticity and connectivity. SNAP25 could regulate glutaminase (GLS)-mediated glutaminolysis, and GLS knockdown could rescue the anti-tumors effect of this protein in glioma cells. Thus, this protein can regulate cancer progression [21,22]. The SBVS is applied to several drugs for brain tumors, that are selected from two databases, that is, PubChem and DrugBank. Thus, in this research, we performed a docking-based virtual screening approach by using PyRx 0.8 tool. The aim was to identify new SNAP25 protein inhibitors with high binding affinity. The top-ranked compounds were then submitted to another screen by using AutoDock 1.5.6.

METHODS

Protein structure preparation

The fasta format sequence of the mutated protein, SNAP25 (ID-P60880) was collected from UniProtKB Database [23]. This was modeled with the help of the I-TASSER online server [24].

This online server helps in developing computational methods to predict the 3-D structure of protein molecules from the amino acid sequence and to deduce the biological functions based on the sequence-to-structure-to-function paradigm. After modeling the proteins, PredictSNP was performed to see the percentage of amino acid mutations. Amino acid with maximum mutation for the brain tumors was selected for further analysis in this case. Therefore, the mutation chosen in this case is Q116A [25]. Thus, the mutation was performed for the protein with the help of the visualization tool PyMOL (2.5) and saved in PDB format for further analysis (Fig. 1) [26]. This molecular graphic tool has been used for 3D visualization of macromolecules. The utilities of the PyMOL tool have been extensively enhanced by various

plugins, including macromolecular analysis, homology modeling, protein-ligand docking, and pharmacophore modeling. Furthermore, Ramachandran Plot was prepared for mutated SNAP25 using the Ramachandran Plot- ZLab tool to study the secondary structure of the protein (Fig. 2).

Dataset collection and preparation

To identify the potential drugs against mutated SNAP25, data regarding 17 drugs effective in the case of brain tumors, to be used as ligands were collected from PubChem and DrugBank database [27,28] (Table 1). Following ligands were used in this computational research: Carmustine, Citicoline, Cyclophosphamide, Etoposide, Lomustine, Mannitol, Methotrexate, Temozolomide, Belzutifan, Merizomib, Indoximod, Galunisertib, Etanidazole, Bafetinib, Glasdegib, Crenolanib, and Methfuroxam.

Further, SwissADME was performed by adding the SMILES of these ligands to it. ADME parameters were analyzed [29] and Lipinski Rule-of-five was performed on these ligands to see whether they are capable of being a potent drug or not [30] (Table 2). The selected drugs, which in this case were all 17 ligands were imported into OpenBabel within the PyRx 0.8 tool [31] and subjected to energy minimization. These minimized compounds were then transformed into PDBQT format for further analysis.

SBVS

To identify new potent drugs, an SBVS using docking simulations was performed on all the selected 17 ligands for the protein. The mutated SNAP-25 modeled structure was used as a receptor for these ligands. The calculation of binding energies was performed using PyRx. First, a grid box was set to cover the active site of the crystal structure with the following dimensions for protein SNAP25 in °A: center (X, Y, Z) (95.40, 93.92, 102.09), dimensions (X, Y, Z) (48.28, 46.51, 142.28) with an exhaustiveness of 8. The top-ranked compounds were then submitted to another screen by using AutoDock 1.5.6. After loading the PDB form of protein in AutoDock, editing was done by deleting the water molecules and adding polar hydrogen molecules and Kollman charges. Similarly, in the case of selected ligands, the torsion tree parameters

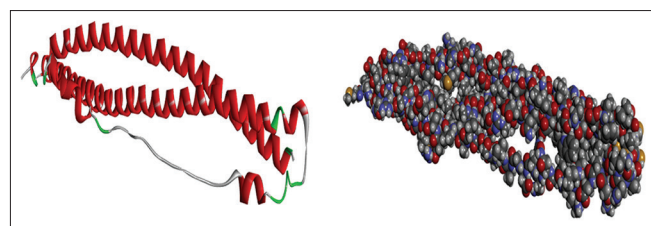


Fig. 1: Mutated protein SNAP25

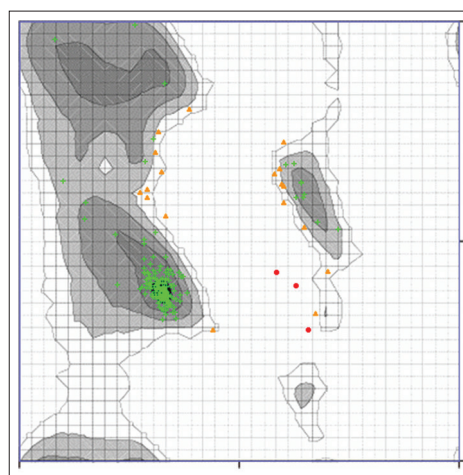


Fig. 2: Ramachandran plot for mutated SNAP25 protein

Table 1: List of ligands and their structures

PubChem Acc. ID	Ligand name	Molecular formula	Molecular weight	Molecular refractivity	No. of H bond acceptor	No. of H bond donor
CID 2578	Carmustine	C5H9Cl2N3O2	214.05g/mol	46.77	3	1
CID 13804	Citicoline	C14H26N4O11P2	488.32 g/mol	102.47	12	4
CID 2907	Cyclophosphamide	C7H15Cl2N2O2P	261.09 g/mol	62.6	4	1
CID 36462	Etoposide	C29H32O13	588.56 g/mol	139.11	13	3
CID 3950	Lomustine	C9H16ClN3O2	233.70 g/mol	59.08	3	1
CID 6251	Mannitol	C6H14O6	182.17 g/mol	37.93	6	6
CID 126941	Methotrexate	C20H22N8O5	454.44 g/mol	118.4	9	5
CID 5394	Temozolomide	C6H6N6O2	194.15 g/mol	44.4	5	1
CID 117947097	Belzutifan	C17H12F3NO4S	383.34 g/mol	84.61	8	1
CID 11347535	Marizomib	C15H20ClNO4	313.78 g/mol	81.64	4	2
CID 405012	Indoximod	C12H14N2O2	218.25 g/mol	62.26	3	2
CID 10090485	Galunisertib	C22H19N5O	369.42 g/mol	108.18	4	1
CID 3276	Etanidazole	C7H10N4O4	214.18 g/mol	50.9	5	2
CID 11387605	Bafetinib	C30H31F3N8O	576.62 g/mol	158.18	10	2
CID 25166913	Glasdegib	C21H22N6O	374.44 g/mol	111.53	4	3
CID 10366136	Crenolanib	C26H29N5O2	443.54 g/mol	132.96	5	1
CID 34313	Methfuroxam	C14H15NO2	229.27 g/mol	67.82	2	1

Table 2: ADME parameters for ligands

Ligand name	Log Po/w (iLOGP)	Log Po/w (WLOGP3)	Log Po/w (WLOGP)	Log Po/w (MLOGP)	Log Po/w (SILICOS-IT)	LIPINSKI-likeness
Carmustine	1.72	1.53	1.16	0.99	0.66	Yes; 0 violation
Citicoline	-4.09	-3.93	-1.48	-6.78	-4.06	Yes ; 1 Violation : Nor O>10
Cyclophosphamide	1.92	0.63	1.5	0.97	1.13	Yes; 0 violation
Etoposide	3.31	0.6	1.01	-0.14	0.95	No; 2 violations: MW>500, Nor O>10
Lomustine	2.36	2.83	2.25	1.55	1.04	Yes; 0 violation
Mannitol	0.34	-3.1	-3.59	-2.77	-1.91	Yes; 1 violation: NH or OH>5
Methotrexate	1.01	-1.85	0.13	-1.13	-0.66	Yes; 1 violation: Nor O>10
Temozolomide	1.29	-1.06	-2.08	-0.98	-1.78	Yes; 0 violation
Belzutifan	2.15	2.02	4.98	2.21	3.04	Yes; 0 violation
Marizomib	2.1	1.81	0.75	1.44	2.33	Yes; 0 violation
Indoximod	1.56	-1.33	1.13	-1.38	0.98	Yes; 0 violation
Galunisertib	2.75	2.39	3.51	1.84	3.69	Yes; 0 violation
Etanidazole	0.61	-1.34	-1.1	-1.7	-2.58	Yes; 0 violation
Bafetinib	4.16	4.18	5.82	2.52	4.28	Yes; 1 violation: MW>500
Glasdegib	2.41	2.37	2.5	1.64	2.07	Yes; 0 violation
Crenolanib	3.49	3.69	3.54	2.24	3.21	Yes; 0 violation
Methfuroxam	2.55	2.99	3.27	2.04	3.46	Yes; 0 violation

were set. Then, just like PyRx, grid box dimensions were set and saved, and grid.gpf file was saved for each ligand. Auto grid script was run and grid.glg file was created. After the successful completion of the auto grid, the docking process was performed by saving the dock.dpf file. Later, the AutoDock script was run and dock.dlg file was created. The completion of this process led to the analysis of the result by saving the first model of the ligand-protein binding conformation in PDB format, ranked by energy. Finally, an analysis of the finding was performed using Discovery Studio [32] and PyMOL [33] programs.

Molecular dynamic simulation

The best-hit compound was subjected to dynamic studies to monitor the stability of the compound followed by the root mean square deviation (RMSD) and root mean square fluctuation (RMSF) graphs [34]. We have used the GROMOS96 54a7 force field through the GROMACS package for molecular dynamic simulation in Linux operating system with GUI. A prodrug server was used to prepare the protein topologies and GROMOS96 54a7 force field with respect to simulation files using the standard parameters. The simulation run was for 100 ns to prepare the graph ratio followed by MMPBSA for the last 50 ns for the accuracy of the results.

RESULTS AND DISCUSSION

Ramachandran plot

To study the secondary structure of our protein, we performed the Ramachandran Plot to know the highly preferable areas covering the

proteins with the help of the Ramachandran Plot-Zlab tool. In the plots, we can predict the distribution of amino acid backbone conformations in peptide and protein structures. Every amino acid residue in a polypeptide can have a specific set of ϕ and ψ angles, therefore, each residue can be represented as a point on this plot with corresponding ϕ and ψ angles as x and y coordinates, respectively. Polypeptides, when adopting secondary structures, rotate at specific torsional angles each time to form regular repetitive structures such as α -helix and β -sheet. Therefore, on plotting these torsional angles to the Ramachandran plot, we obtain, a very restricted area on the plot which can be used to identify and check the secondary structure in a given polypeptide. The backbone torsion angles for right-handed α -helix are approximately $\phi = -57^\circ$ and $\psi = -47^\circ$ and therefore, occupy the small area on the lower-left quadrant. β -the sheet is made up of almost fully extended strands, with ϕ and ψ angles falling in the upper-left quadrant of the Ramachandran plot.

Amino acids mentioned with the green color are used to make the majority of the protein and black and grey colors are predicting ones that make the best structure of the protein. The fourth quadrant is the non-allowed region and if amino acids are found in this part, then, it will be either orange or red, as mentioned in the graphs below. These amino acids falling in the fourth quadrant are not used to make any major part of the protein (Fig. 2) [35]. As shown in the figure, the protein has a maximum number of amino acids falling under the preferable zone. The protein is mainly made of alpha-helical and beta sheets. As predicted by

the plots, SNAP25 protein has 88.889% of amino acids are in the highly preferable zone, 9.524% in the preferred area, and the rest 1.587% in a non-preferred zone.

SBVS

To find new potentially approved drugs for treating brain tumors, SBVS was performed for all 17 ligands for both proteins. PyRx tool generated nine different conformations for each ligand which are classified by binding affinity (kcal/mol). The first model of the ligand-protein binding conformation was saved in PDB format and studied in PyMOL. The 17 compounds for the mutated protein, displaying the free energy of binding are presented in the table below. Only, the top-ranked compounds with a binding affinity ranging between -7.0 and -9.8 kcal/mol were selected for further process.

The top hit selected six ligands including etoposide, methotrexate, galunisertib, bafetinib, glasdegib, and crenolanib has shown binding energy >-7.0 kcal/mol and <-9.8 kcal/mol for mutated SNAP25 were selected for autodocking (Table 3, Figs. 3 and 4).

Thus, these ligands have been submitted to AutoDock 1.5.6 tool, separately, for both the proteins and the binding energies were calculated again to know the best results for these mutated proteins. The results were saved in PDB format and analysis was done with the help of PyMOL and the Discovery studio online server. As shown in the above table, ligand crenolanib and etoposide have the best binding energy results to form a ligand-receptor bond.

Molecular dynamic simulation

The calculated molecular docking results were subjected to the molecular dynamic simulation using GPU enabled GROMACS package. Ligand topology was generated using the Prodrug server followed by adding the default parameters. Initially, GROMACS was used to set the system preparation for 1500 steps using the steepest descent algorithm and put it into the cubic periodic box with an SPCE water model. The dynamic system was complementarily maintained with a standard salt concentration of 0.15 M by adding Na^+ and Cl^- counter ions. In terms of NPT equilibration, the phase was subjected to a final production run for 100 ns simulation time and RMSF and RMSD graph was generated using trajectory files and standard parameters.

To formulate new drugs, molecular dynamics studies are mostly carried out to evaluate complexation. The RMSD graph defines the positional divergence of one or more atoms (Fig. 5) and depicts the average deviation as noticed between the corresponding atoms of the

proteins, whereas the RMSF plot represents the extent of the positional variance of a specific atom over time (Fig. 6). The alteration in structural compression is reflected by the radius of the gyration graph (Fig. 7). As observed in Fig. 7, the protein maintains its compression all across the simulation time, and no pronounced peaks or declines

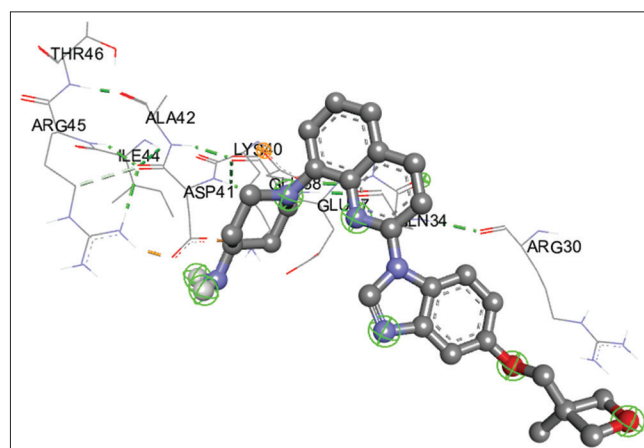


Fig. 3: Crenolanib interaction with SNAP25 amino acids (THR 46, ALA42, ARG 45, ILE 44, ASP41, ARG30)

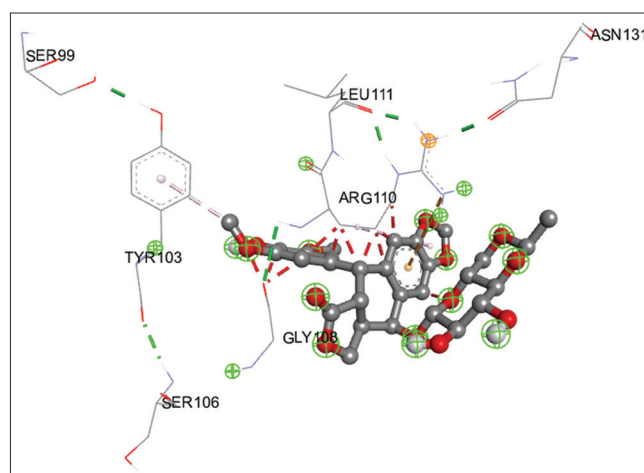


Fig. 4: Etoposide interaction with SNAP25 amino acids (LEU11, SER99, TYR103, SER106, GLY108, ARG110)

Table 3: Binding energy (kcal, mol) for ligands in PyRx and AutoDock tool

Anticancer drugs	Binding affinity towards SNAP-25
Carmustine	-4.2
Citicoline	-5.9
Cyclophosphamide	-4.4
Etoposide	-7.7
Lomustine	-5.3
Mannitol	-4.4
Methotrexate	-7.4
Temozolomide	-5.6
Belzutifan	-6.6
Marizomib	-6.3
Indoximod	-6
Galunisertib	7.5
Etanidazole	-4.9
Bafetinib	-8.1
Glasdegib	-7.5
Crenolanib	-7.7
Methfuroxam	-6.5

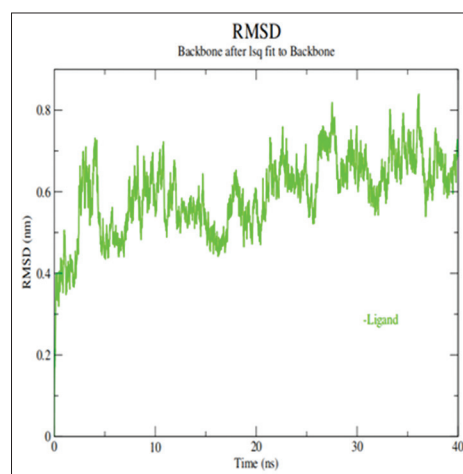


Fig. 5: Root mean square deviation

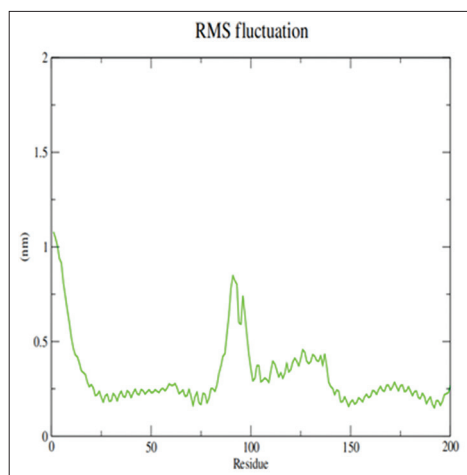


Fig. 6: Root mean square fluctuation

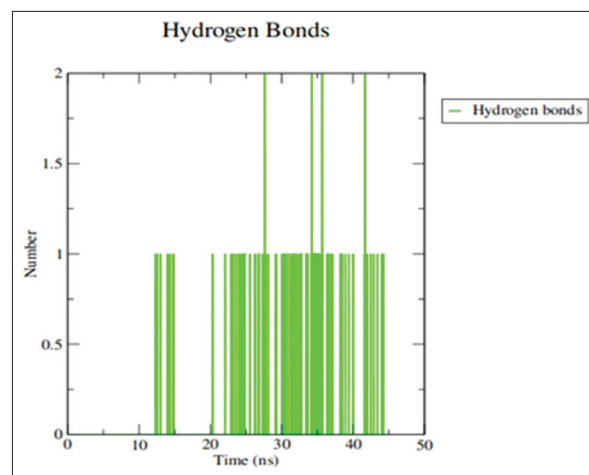


Fig. 9: H-bond interactions

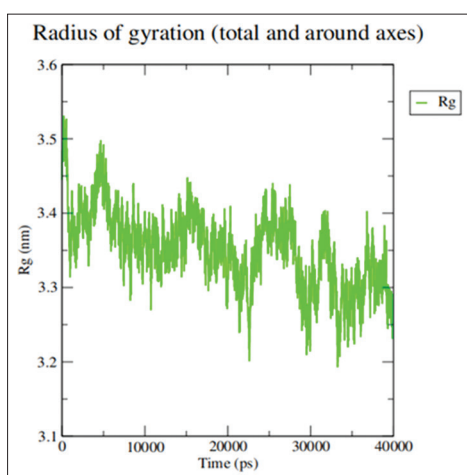


Fig. 7: Radius of gyration

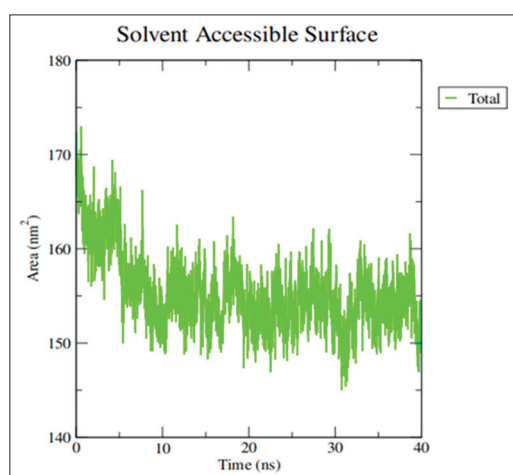


Fig. 8: Solvent accessible surface area

were seen, suggesting that the structures did not experience any significant structural changes. The solvent accessible surface area plots indicate the entire region of the protein that is accessible to the ligand molecule (Fig. 8). The primary driver behind the drug's action is the ligand's binding to the protein's active or allosteric region. In addition, hydrogen bonds are frequently used to stabilize the binding modes (Fig. 9).

CONCLUSION AND INTERPRETATION

In this study, initially, the mutated protein, selected from UniProtKB, and all 17 ligands were prepared for the SBVS process. Modeling of protein was done to delete all the extra molecules attached to it and to make it accessible for the autodocking process. With the help of PredictSNP, the protein was analyzed for the maximum mutations responsible for the disease, and only one, highly mutated amino acid was selected to proceed further with our research. PyMOL was used to mutate the protein and then, it was used for preparing the Ramachandran Plot. Maximum amino acid residues fall under the allowed area making it preferable to use i.e. 97% for SNAP25. Similarly, these 17 ligands, which were selected with the help of PubChem and DrugBank databases, were used to perform SwissADME to create their structures and to study their properties with ADME parameters. Furthermore, the LIPINSKI Rule of Five was applied to them to check whether they could make a potent drug to use. The results were favorable for all these ligands. Thus, a SBVS was applied on 17 ligands using PyRx 0.8 software and binding affinity for each one of these compounds was calculated for the mutated protein. The first model of the protein-ligand conformations was saved in PDB format to check the results in PyMOL. Based on the highest binding free energy ($>-7.0\text{kcal/mol}$ to $<-9.8\text{kcal/mol}$), six ligands, that is, etoposide, methotrexate, galunisertib, bafetinib, glasdegib, and crenolanib were then verified by using AutoDock (1.5.6) tools for their binding efficacy towards the mutated SNAP-25 protein. Among these, Crenolanib exhibited the highest binding affinity along with strong and stable interactions for SNAP25 (Fig. 3) as validated by the molecular dynamic simulation studies (Figs. 5-9). From the findings of the current study, it can be hypothesized that the investigational drug Crenolanib is a potent inhibitor for the mutated SNAP25 protein and exerts cancer modulatory potential.

ACKNOWLEDGMENT

I thank Mr Sameer Sharma and Vaeshnavi Buwa, BioNome, Bioinformatics to provide the guidance in the research project.

REFERENCES

- Gilbert MR, Dignam JJ, Armstrong TS, Wefel JS, Blumenthal DT, Vogelbaum MA, *et al.* A randomized trial of bevacizumab for newly diagnosed glioblastoma. *N Engl J Med* 2014;370:699-708.
- Chinot OL, Wick W, Mason W, Henriksson R, Saran F, Nishikawa R, *et al.* Bevacizumab plus radiotherapy-temozolomide for newly diagnosed glioblastoma. *N Engl J Med* 2014;370:709-22.
- Smith MA, Reaman GH. Remaining challenges in childhood cancer and newer targeted therapeutics. *Pediatr Clin North Am* 2015;62:301-12.
- Phoenix TN, Patmore DM, Boop S, Boulos N, Jacus MO, Patel YT, *et al.* Medulloblastoma genotype dictates blood brain barrier phenotype. *Cancer Cell* 2016;29:508-22.

5. Gerstner ER, Fine RL. Increased permeability of the blood-brain barrier to chemotherapy in metastatic brain tumors: Establishing a treatment paradigm. *J Clin Oncol* 2007;25:2306-12.
6. Mackay A, Burford A, Carvalho D, Izquierdo E, Fazal-Salom J, Taylor KR, *et al.* Integrated molecular meta-analysis of 1,000 pediatric high-grade and diffuse intrinsic pontine glioma. *Cancer Cell* 2017;32:520-37.
7. Quail DF, Joyce JA. The microenvironmental landscape of brain tumors. *Cancer Cell* 2017;31:326-41.
8. Gilbertson RJ. Mapping cancer origins. *Cell* 2011;145:25-9.
9. Xia L, Su X, Shen J, Meng Q, Yan J, Zhang C, *et al.* ANLN functions as a key candidate gene in cervical cancer as determined by integrated bioinformatic analysis. *Cancer Manag Res* 2018;10:663-70.
10. Yuan L, Zeng G, Chen L, Wang G, Wang X, Cao X, *et al.* Identification of key genes and pathways in human clear cell renal cell carcinoma (ccRCC) by co-expression analysis. *Int J Biol Sci* 2018;14:266-79.
11. Aissouq AE, Toufik H, Stitou M, Ouammou A, Lamchouri F. *In silico* design of novel tetra-substituted pyridinylimidazoles derivatives as c-jun N-terminal kinase-3 inhibitors, using 2D/3D-QSAR studies, molecular docking and ADMET prediction. *Int J Pept Res Ther* 2020;26:1335-51.
12. Song CM, Lim SJ, Tong JC. Recent advances in computer-aided drug design. *Brief Bioinform* 2009;10:579-91.
13. Macalino SJ, Gosu V, Hong S, Choi S. Role of computer-aided drug design in modern drug discovery. *Arch Pharm Res* 2015;38:1686-701.
14. Gangwal RP, Dhoke GV, Damre MV, Khandelwal K, Sangamwar AT. Structure-based virtual screening and molecular dynamic simulation studies to identify novel cytochrome bc1 inhibitors as antimalarial agents. *J Comput Med* 2013;2013:637901.
15. Srinivasan P, Perumal PC, Sudha A. Discovery of novel inhibitors for Nek6 protein through homology model assisted structure based virtual screening and molecular docking approaches. *ScientificWorldJournal* 2014;2014:967873.
16. Wang Y, Han R, Zhang H, Liu H, Li J, Liu H, *et al.* Combined ligand/structure- based virtual screening and molecular dynamics simulations of steroidal androgen receptor antagonists. *BioMed Res Int* 2017;2017:3572394.
17. Wang W, Wan D, Liao D, Peng G, Xu X, Yin W, *et al.* Identification of potent chloride intracellular channel protein 1 inhibitors from traditional Chinese medicine through structure-based virtual screening and molecular dynamics analysis. *BioMed Res Int* 2017;2017:4751780.
18. Liu Z, Zhao J, Li W, Wang X, Xu J, Xie J, *et al.* Molecular docking of potential inhibitors for influenza H7N9. *Comput Math Methods Med* 2015;2015:480764.
19. Dubey R, Tewari AK, Singh VP, Singh P, Dangi JS, Puerta C, *et al.* Molecular docking study of conformational polymorph: Building block of crystal chemistry. *ScientificWorldJournal* 2013;2013:309710.
20. Zhang D, Hu Y, Sun Q, Zhao J, Cong Z, Liu H, *et al.* Inhibition of transforming growth factor beta-activated kinase 1 confers neuroprotection after traumatic brain injury in rats. *Neuroscience* 2013;238:209-17.
21. Guo C, Zhuang Y, Chen Y, Chen S, Peng H, Zhou S. Significance of tumor protein p53 mutation in cellular process and drug selection in brain lower grade (WHO grades II and III) glioma. *Biomark Med* 2020;14:1139-50.
22. Huang Q, Lian C, Dong Y, Zeng H, Liu B, Xu N, *et al.* SNAP25 Inhibits glioma progression by regulating synapse plasticity via GLS-mediated glutaminolysis. *Front Oncol* 2021;11:698835.
23. UniProt Consortium. UniProt: A worldwide hub of protein knowledge. *Nucleic Acids Res* 2019;47:D506-15.
24. Roy A, Kucukural A, Zhang Y. I-TASSER: A unified platform for automated protein structure and function prediction. *Nat Protoc* 2010;5:725-38.
25. Bendl J, Stourac J, Salanda O, Pavelka A, Wieben ED, Zendulka J, *et al.* PredictSNP: Robust and accurate consensus classifier for prediction of disease-related mutations. *PLoS Comput Biol* 2014;10:e1003440.
26. Yuan S, Chan HC, Hu Z. Using PyMOL as a platform for computational drug design. *WIREs* 2017;7:e1298.
27. Wishart DS, Feunang YD, Guo AC, Lo EJ, Marcu A, Grant JR, *et al.* DrugBank 5.0: A major update to the drug bank database for 2018. *Nucleic Acids Res* 2018;46:D1074-82.
28. Kim S, Chen J, Cheng T, Gindulyte A, He J, He S, *et al.* PubChem in 2021: New data content and improved web interfaces. *Nucleic Acids Res* 2021;49:D1388-95.
29. Tian S, Wang J, Li Y, Li D, Xu L, Hou T. The application of *in silico* drug-likeness predictions in pharmaceutical research. *Adv Drug Deliv Rev* 2015;86:2-10.
30. Lipinski CA, Lombardo F, Dominy BW, Feeney PJ. Experimental and computational approaches to estimate solubility and permeability in drug discovery and development settings. *Adv Drug Deliv Rev* 2001;46:3-26.
31. Dallakyan S, Arthur JO. Small-molecule library screening by docking with PyRx. *Methods Mol Biol* 2015;1263:243-50.
32. BIOVIA-Scientific Enterprise Software for Chemical Research. Material Science R&D; 2020. Available from: <https://www.3dsbiovia.com> [Last accessed on 2022 Dec 27].
33. Lilkova E. The PyMOL Molecular Graphics System, Version 2.2.0. New York: Schrödinger LLC; 2015.
34. Hollingsworth SA, Dror RO. Molecular dynamics simulations for all. *Neuron* 2018;99:1129-43.
35. Ramachandran GN, Ramakrishnan C, Sasisekharan V. Stereochemistry of polypeptide chain configurations. *J Mol Biol* 1963;7:95-9.